2021

Linear Generators in Wave Energy Conversion: Performance, Feasibility, and Location Study

Luis Fernandez de Valderrama
University of North Florida, n01444166@unf.edu

Linear Generators in Wave Energy Conversion:

Performance, Feasibility, and Location Study.

Luis Fernandez de Valderrama

College of Computing, Engineering, and Construction

University of North Florida

April 2021

Sponsored by

Taylor Engineering Research Institute (TERI)

Chairperson of the Supervisory Committee:

Professor Cigdem Akan

Department of Civil Engineering

Members of the Supervisory Committee:

Professor Don Resio

Department of Civil Engineering

Professor Brian Kopp

Department of Electrical Engineering

Thesis entitled "Linear Generators in Wave Energy Conversion: Performance, Feasibility, and Location Study." by Luis Fernandez de Valderrama is approved:

Committee Chair: Dr. Cigdem Akan

Committee Member: Dr. Don Resio

Committee Member: Dr. Brian Kopp

Accepted for the School of Engineering:

Department Chair: Dr. Osama Jadaan

Accepted for the University:

Dean of the Graduate School: Dr. John Kantner

Table of Contents

List of Figures

Abstract

As the energy demand increases and climate change becomes a major problem, the solution to decrease greenhouse gas emissions and mitigate the effects of climate change involves increasing the use of sustainable and renewable sources to generate electricity. However, developed renewable sources have inconveniences that make them incapable of generating the totality of the electricity that a country demands. Wave energy is an alternative renewable energy source that can help mitigate the inconveniences of other renewable sources and decrease the emission of greenhouse gases.

This study aims to find the potential of linear generators in wave energy by analyzing the output based on different wave conditions. The study uses a numerical simulation verified by experimental data to optimize the output of the linear generator. Based on the current results, it can be stated that adding magnets increases the output, and that the maximum output greatly varies based on the coil configuration. The main external factor that improves the output is a short wave period.

Linear Generators in Wave Energy Conversion: Performance, Feasibility, and Location Study

1 Introduction

Due to the increasing world population and technological developments, worldwide energy demand has increased in the past decades. The primary sources of energy generation in the United States are oil and natural gas (EIA, 2019). Both sources have limited availability, and emit carbon dioxide into the atmosphere. Carbon dioxide emissions cause rising temperatures, melting ice caps, and increased frequency of extreme weather conditions. This has encouraged governments to reduce carbon dioxide emissions by, among other actions, attempting to gradually switch to renewable sources to generate electricity with the goal of fully renewable energy generation.

1.1 Renewable Energy

The production of renewable energy has increased exponentially in the United States (EIA, 2019). The main renewable sources used in the United States that do not emit harmful gases to the atmosphere are wind energy, hydroelectric, and solar. These three sources provided 6% of the total energy consumed in the United States in 2019 (EIA, 2019). Even though this may look like a small amount, the same sources provided less than 0.01% of the total energy consumed in 2009 (EIA, 2009). Therefore, there has been a significant increase in the usage of renewable sources in the last decade. Moreover, it is intended to continue increasing the use of renewable sources to generate electricity.

However, these sources have some limitations in their use. Hydroelectric power is limited to very specific locations that are suitable for the construction of dams. These are also very expensive to build and have a great impact on the watercourse wildlife. The wind is a very

intermittent source of energy. Also, the air has a low density and therefore needs big and numerous turbines to generate significant amounts of energy, which takes up much space. Last, solar energy uses solar panels that take much space inland. It is also restricted to latitudes where sunlight is most common, and produces no energy at night or during very cloudy and rainy days, making it, similarly to the wind, an intermittent energy source.

Aiming to expand renewable energy and get closer to completely clean energy generation, interest in wave energy has increased in recent years. Oceans cover about 70% of the Earth's surface, water has a density nearly 850 times higher than air, and nearly 30% of the United States population live in coastal counties (US Census Bureau, 2020). These make waves a very attractive source of energy.

1.2 Wave Energy

Waves have a theoretical global potential of 32000 TWh/yr (IPCC, 2012), with more than 2500 TWh/yr incident on the coasts of the United States (U.S. Department of Energy, 2019). Waves are very consistent, although seasonal and synoptic-scale variations can be significant. Thus, wave energy could be a great addition to the intermittence of solar and wind energy. These make wave energy important for decreasing the dependability in sources that emit greenhouse gases and a cornerstone for transitioning to fully sustainable and renewable energy production.

Given the potential of wave energy, there are numerous research efforts focused on developing wave energy technology. There are many wave energy converter patents, but few commercialized wave energy converters connected to the grid (Aderinto, 2018). Some of the main barriers to the development of wave energy are the lack of development in technology, the

uncertainty surrounding the impact of wave farms on the coast and the marine life, and the high initial investment (Astariz, 2015).

The industry is facing both technological and economic challenges when developing wave energy converters. The technologies used for wave energy conversion are still in the infancy of their development stage compared to the technologies used for other renewable energies like wind or solar. For building and deploying a wave energy converter the initial cost is very high, and due to the harsh conditions of the ocean, the operating costs also remain high. That leads to an elevated cost of energy, dissipating the interests of potential investors. Therefore, more research and technology development are required to lower the cost of wave energy and make it economically attractive.

According to their deployment location, wave energy converters may be classified as onshore, nearshore, and offshore devices. Waves have greater energy in offshore locations. However, the conditions at these locations tend to be more severe. Because of that, offshore locations require a higher initial investment and cost of operation.

According to the conversion principle, there are four main categories of wave energy converters: oscillating water column, overtopping devices, point absorbers, and wave-activated bodies (Koca, 2013).

Oscillating water column devices are partially submerged hollow structures that enclose air. As the waves pass by, the air enclosed gets compressed and passes through a turbine to generate electricity (Koca, 2013).

Overtopping devices are floating structures that concentrate the waves into a sloping ramp where there is a reservoir over the mean water level of the surrounding sea. Then, the water passes through a turbine to return to the sea (Liu, 2017).

W**ave-activated bodies** have moving elements that are activated by the oscillating motion of the waves. These devices operate parallel to the wave direction and capture energy from the relative motion between different device parts.

Last, **point absorbers** are buoy-type converters that use the up-down motion of the waves to generate electricity. Point absorbers may use different types of energy conversion systems, including linear generators. This study is focused on a point absorber that uses a linear generator to covert the energy from the waves.

1.3 Linear Generators

Linear generators are used in applications that involve linear motions to reduce mechanical complexity. Their use in wave energy conversion was introduced relatively recently. However, most recently developed wave energy converters use hydraulic systems to spin turbines attached to generators. One of the reasons for this is that hydraulic power take-off is more suitable for slow motions with high strength (Polinder, 2007).

However, the lower maintenance requirements as well as their higher reliability due to the need for fewer mechanical components, are drawing attention from the wave energy community towards linear generators. Even though they may be used in larger converters, linear generators are an attractive option for harvesting power from the waves in smaller devices, with ratings lower than the MW (Simone, 2014). As a result, several studies focused on estimating

and improving the power output using linear generators in different wave energy converter designs and prototypes.

One example of wave energy converter that uses a linear generator is the Archimedes Wave Swing, developed by Teamwork Technology BV of Netherlands. This device has an end fixed to the seafloor and an oscillating part called “floater”. Using the differences in pressure generated by waves, the floater moves up in wave troughs and down in wave crests. This motion is resisted by a linear electrical generator, generating electricity. The Archimedes Wave Swing was the first wave energy converter to use a linear generator. A prototype was built in Portugal, and it is rated at 2MW of maximum instantaneous power and a unit power of 2000 kW (Poullikkas, 2014).

Another example of a wave energy converter that uses a linear electrical generator is the Swedish Buoy, also called Lysekil Project. This device has a unit power under 100 kW and uses a three-phase permanent magnet linear generator placed on the seabed connected to a heaving buoy to generate electricity (Poullikkas, 2014).

2 Objectives

This study aims to set the foundation for developing a wave energy converter that uses linear generators to convert wave energy into electrical energy. Specific goals of this study are:

1. To evaluate the influence of the magnets and the coil configuration in the output.
2. To optimize the magnets and the coil configuration in the wave energy converter.
3. To perform case studies at different locations and determine which locations are more suitable for this energy conversion type.

3 Methods

The wave energy converter of this study is a point absorber that, as the waves pass by, they move a piston with neodymium permanent magnets vertically. Around the piston, there is a stator with a coil in which current is induced by the relative motion of the piston's permanent magnets.

3.1 Numerical Simulation

The output of the wave energy converter was modeled using a numerical simulation. The simulation was done using MATLAB () and Finite Element Method Magnetics (Meeker, 2019), FEMM for short. FEMM is software that uses the Finite Element Method (FEM) to solve electromagnetic problems. FEM is a numerical method that solves complex problems by subdividing the problem domain into smaller and simpler parts that may be solved individually.

The main principle used to solve for the output is Faraday's Law of Electromagnetic Induction shown in (1), which predicts the voltage induced through a coil that experiences a change in magnetic flux, where *N* is the number of loops in the coil, $\Delta\phi$ is the change in magnetic flux, and Δt is the change in time.

$$emf = -N\frac{\Delta\phi}{\Delta t} \tag{1}$$

FEMM and MATLAB were used to calculate the magnetic flux perpendicular to wire loops with radius *r* and vertical distance from the center of the magnet *z*. The loops were assumed to be concentric to the magnets. This magnetic flux was interpolated to any coil loop of radius *r* and distance *z*. A visual representation of a magnetic flux that was used for interpolation may be observed in Figure 3. The magnetic flux was solved individually for each loop of the

coil, converting Faraday's Law of Electromagnetic Induction (1) into (2), where $\phi_{m,n}$ is the change in magnetic flux at coil loop m and time t_n.

$$emf = \frac{\sum_m (\phi_{m,n} - \phi_{m,n-1})}{t_n - t_{n-1}} = \frac{\sum \Delta\phi_m}{\Delta t} \tag{2}$$

To calculate the output generated by a full wave, the time t was discretized into small time intervals Δt, and $\phi_{m,n}$ was calculated at each coil loop m for every t_n based on the n^{th} position of the magnet. The final problem solution is the result of the superposition of every Δt solution. A MATLAB script was written to do this. The script takes as inputs the wave height H, the wave period T, the wire gauge, the inside diameter of the coil, the coil length (in the z-direction), and the outside diameter of the coil. The length of the wire, resistance of the wire, number of loops in the r and z-direction, output voltage, output power, and output current were calculated from these parameters.

The waves were assumed to be monochromatic, unidirectional sinusoids with amplitude $A = \frac{H}{2}$, and the magnets were assumed to move vertically with the wave; however, this concept can be generalized to work with wave spectra as well. The wire resistance R was calculated according to (3), where ρ is the wire resistivity, l is the wire length, and A is the cross-sectional area of the wire.

$$R = \rho \frac{l}{A} \tag{3}$$

The output power was calculated according to (4) and Ohm's Law (5), where P is power, V is voltage, and I is current.

$$P = VI \tag{4}$$

$$V = IR \tag{5}$$

The average power P_{avg} was calculated according to (6).

$$P_{avg} = \frac{\int P\,dt}{t} \tag{6}$$

For the Parameter Evaluation and Coil Configuration sections of this research, the following assumptions were made:

- H = 1 m
- T = 8 s
- Wire diameter = 3.2 mm
- Wire insulation diameter = 5.4 mm
- ρ = 0.0171 Ω mm^2/m
- Coil inside diameter = 0.23 m
- Magnet diameter = 0.2 m
- Magnet thickness = 0.05 m
- Total resistance = 2 · Wire resistance

3.2 Experimental Data

To obtain experimental data, a small-scale prototype of the wave energy converter was built. To do this, a housing was 3-D printed. The housing was hollow to allow the magnets to move through, with an inside diameter of 31 mm, an outside diameter of 37 mm, and two fins of 50 mm diameter, which help set the coil. The coil had 1000 total turns and a length (distance between the fins) of 30 mm. Using the wire diameter, which was 0.42 mm, the number of loops in the longitudinal direction (*z)* and transversal direction (*r*) were estimated. The small-scale prototype is shown in Figure 1.

Figure 1 – Small-scale prototype

The magnets were slid through the housing at different speeds to observe the output voltage induced by the magnet in the coil across a 1 kΩ resistor. This voltage was recorded using an oscilloscope and compared to the voltage obtained using the numerical simulation.

4 Results and Discussion

First, the magnetic field generated by the magnets was evaluated. Figure 2 denotes what the magnetic field looks like for one, three, and six magnets, arranged with the same polarity along the *z*-direction. The left edge of each image is an axis of radial symmetry.

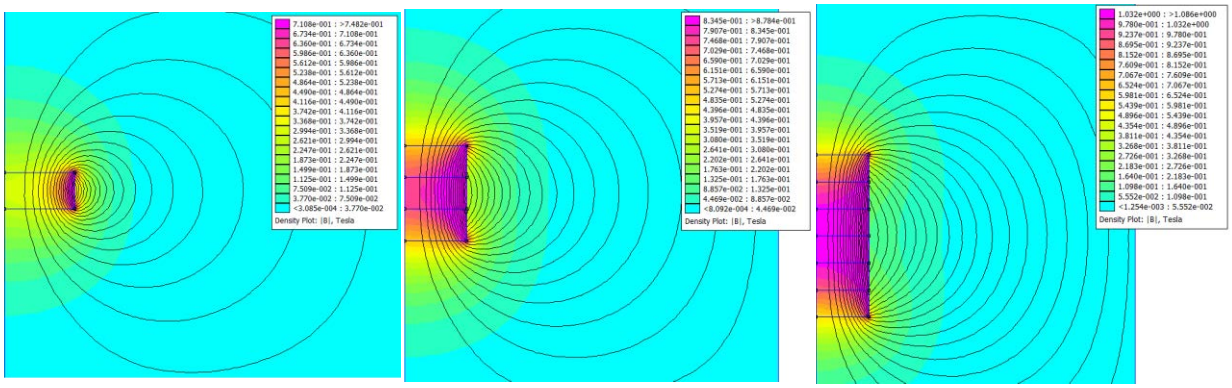

Figure 2 – Magnetic field density and magnetic field lines generated by one, three, and six neodymium magnets arranged with the same polarity along the z-direction. These pictures were generated using FEMM

Figure 2 shows that adding magnets slightly increases the maximum magnetic field density. Also, the areas with the highest density are the magnets themselves, as well as the closest areas to the magnets. The magnetic field lines go through the magnets and from one face to the opposite face of the magnets circularly. According to Figure 2, the highest magnetic flux through the coil should occur when the vertical center of the coil is aligned with the vertical center of the magnets. To confirm this, the magnetic flux of six magnets through a coil loop was plotted in Figure 3.

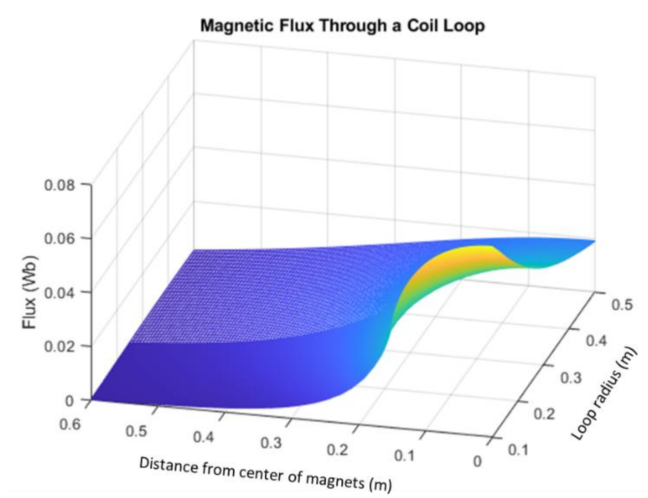

Figure 3 - Flux through a wire loop vs. radius of the wire loop vs. vertical distance from the wire loop to the center of the six magnets

Since the magnetic flux through the wire loops decreases with radius, the inside diameter of the coil must be the smallest possible. Also, Figure 3 confirms that the maximum magnetic flux through the coil happens when the coil center is aligned with the vertical center of the magnets

To evaluate the numerical simulation, experimental data were obtained and compared to the data obtained using the numerical simulation. Figure 4 compares, at different periods, the voltages obtained experimentally and the voltages obtained from the numerical simulation.

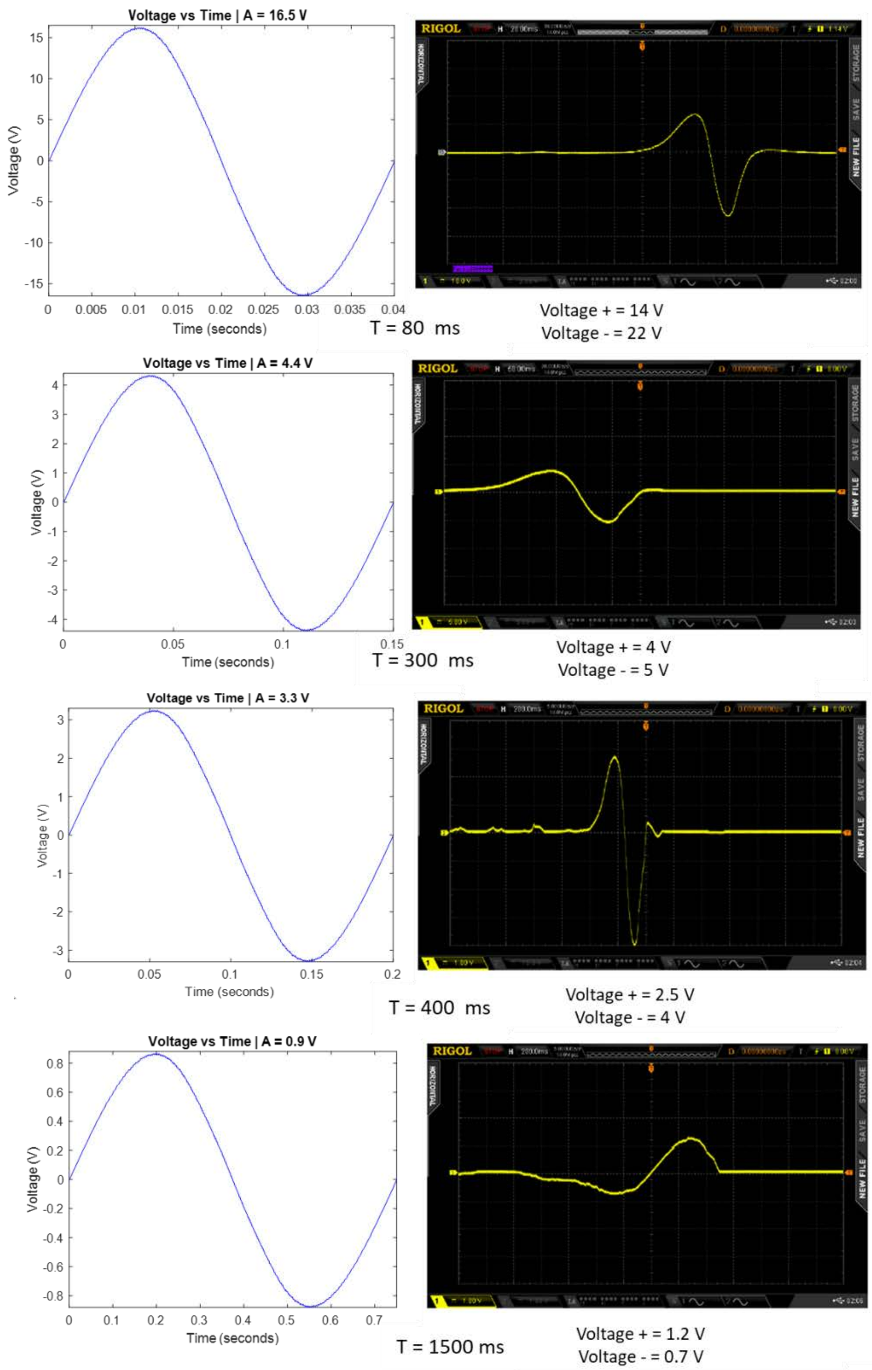

Figure 4 - Voltage comparison of the numerical simulation (left) vs. experimental data (right) at different wave periods

The results in Figure 4 show that the voltage amplitudes obtained using the numerical simulation and the shapes of the waveform are consistent with those obtained experimentally. The difference in sign for period T = 1500 ms is a result of the magnet's polarity being reversed.

Given that the numerical simulation showed realistic results, it was used to evaluate other parameters.

4.1 Parameter Evaluation

The numerical simulation was used to determine how different parameters influence the output. Figure 5 shows how the number of magnets and the length of the coil in the *z*-direction affect the root mean square (RMS) voltage and power. The RMS is the square root of the arithmetic mean of the squares of a set of data, and it is a type of generalized mean that is typically used when the data set has both positive and negative values.

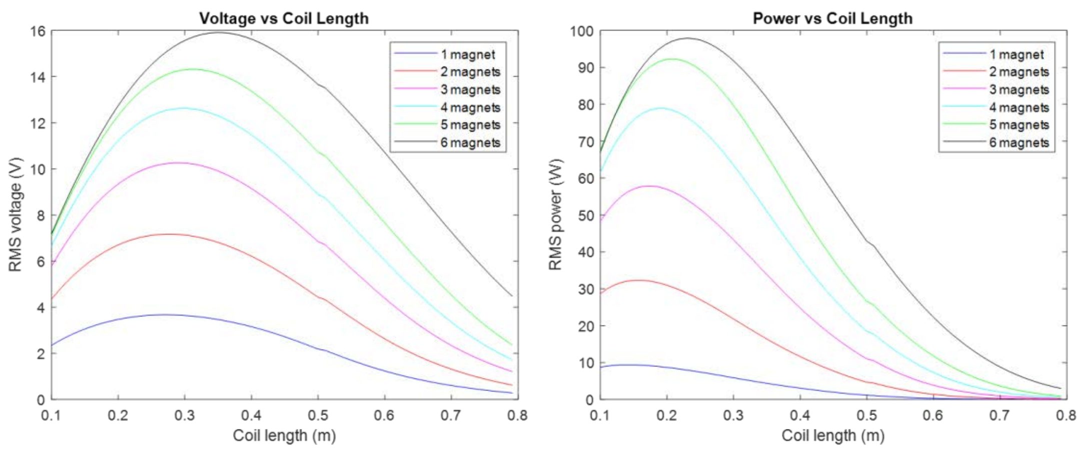

Figure 5 – Output RMS voltage and RMS power vs. coil length in the z*-direction with one through six magnets in the piston*

It can be observed in Figure 5 that adding magnets increases the output nearly linearly, becoming less effective as more magnets are added. Also, it shows that the length of the coil in the *z*-direction affects both voltage and power outputs. Hence, the length of the coil must be carefully chosen to obtain the optimal output based on the conditions. Since the highest output was obtained using more magnets, all subsequent figures were created using six magnets in the

piston unless otherwise specified. The influence of the coil outside diameter (loops in the *r*-direction) in both voltage and power is shown in Figure 6.

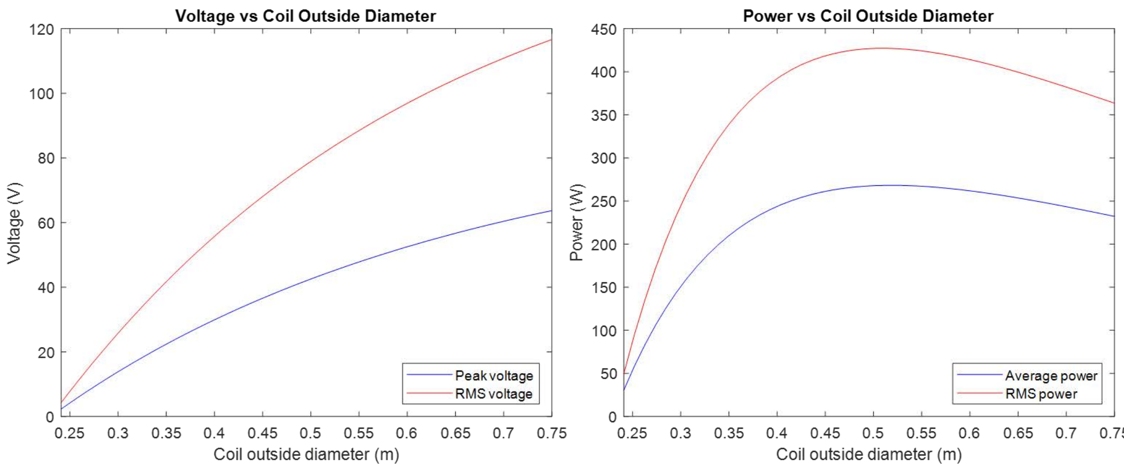

Figure 6 - Output voltage and power vs. number of loops in the transversal direction for six magnets

As exposed in Figure 6, the output voltage increases as the number of loops in the transversal direction increases. However, the output power does not increase indefinitely. This is because even though the voltage increases, the wire resistance increases faster, which decreases the current through the wire and results in reduced output power. Therefore, there is also an optimal number of loops for the transversal direction.

If six magnets were to be used in the wave energy converter, according to Figure 5 and Figure 6, the maximum output would happen at a coil length of 0.25 m and a coil outside diameter of 0.5 m. The voltage and power waveforms for these parameters are shown in Figure 7.

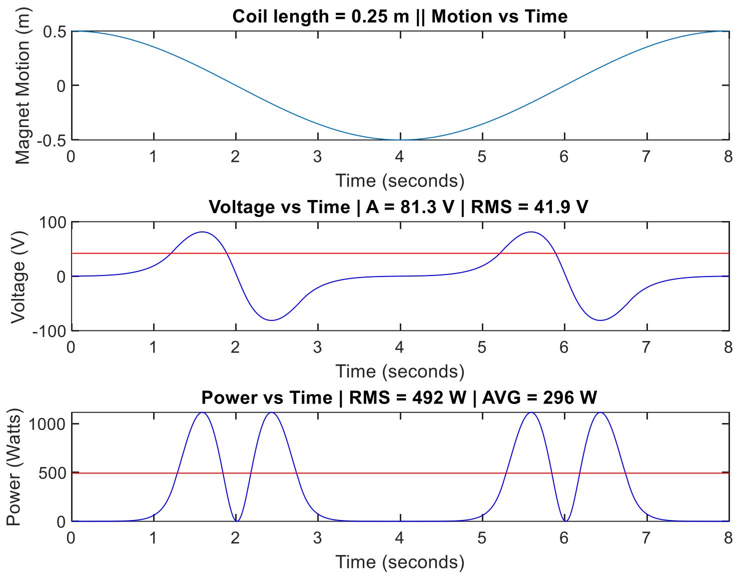

Figure 7 - Voltage and power waveform using six magnets and a coil with 0.25 m in length in the z-direction and 0.5 m of outside diameter

The waveforms shown in Figure 7 have peaks relatively high compared to the rest of the domain, which create a great difference between the RMS or average outputs and the peak values. The main factor that affects the shape of the waveform for a given *H* is the length of the coil. To better understand how the coil length affects the difference between the peak and the RMS voltage, these, together with the ratio of peak to RMS voltage, were plotted against coil length (Figure 8).

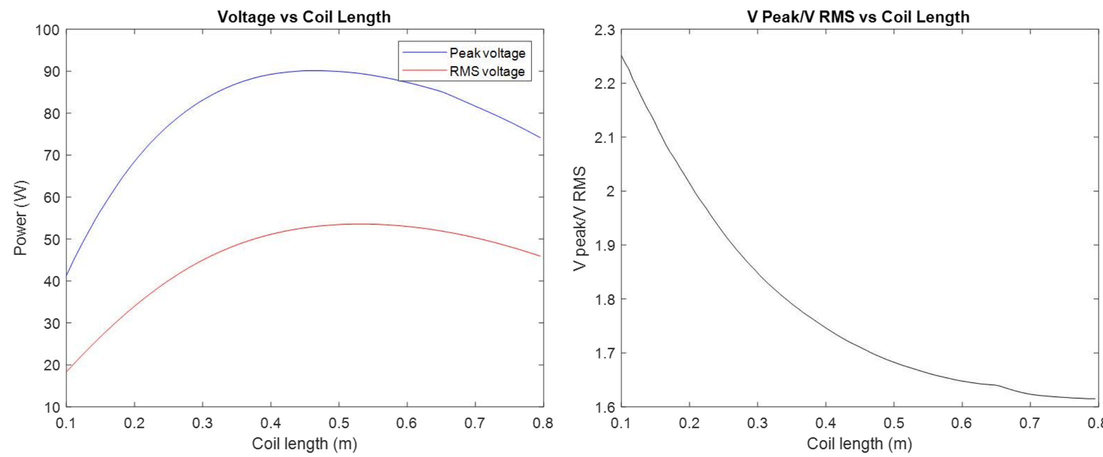

Figure 8 – Peak and RMS voltage vs. coil length. The picture on the right shows the ratio of peak voltage to RMS voltage

According to Figure 8, the ratio of peak to RMS voltage gets reduced as the coil length increases. The waveforms with the highest and lowest ratio of peak to RMS voltage are plotted in Figure 9.

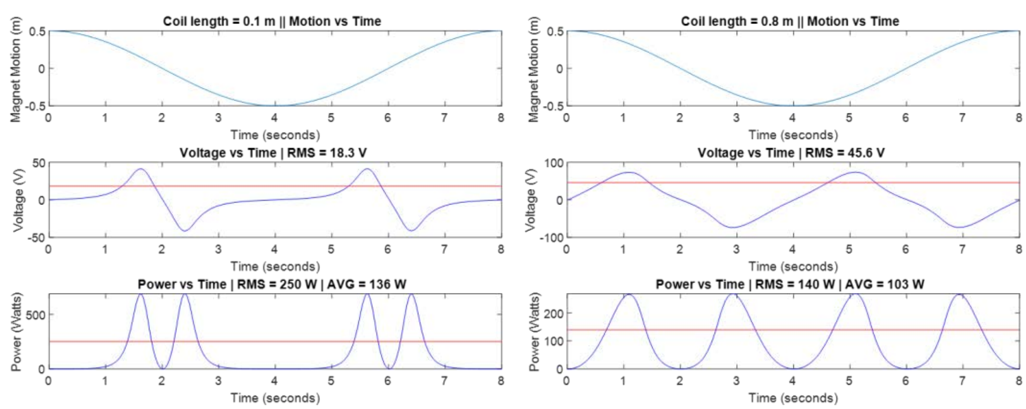

Figure 9 - Voltage and power waveform for the highest and lowest ratio of peak to RMS voltage. The waveform with the highest ratio is shown in the left picture, which happened at a coil length of 0.1 m. The waveform with the lowest ratio is shown in the right picture, which happened at a coil length of 0.8 m

As it can be observed in Figure 9, the waveform for the longer coil is more active throughout the entire domain, as opposed to the waveform with the shorter coil, which has prominent peaks and a great portion of the domain with a negligible output. This becomes more

evident in the power waveform. The maximum average power output was found to be at a coil length of 0.35 m and a coil outside diameter of 0.54 m, where according to Figure 8 the ratio of peak to RMS voltage is about 1.8. The waveform at this coil length is shown in Figure 10.

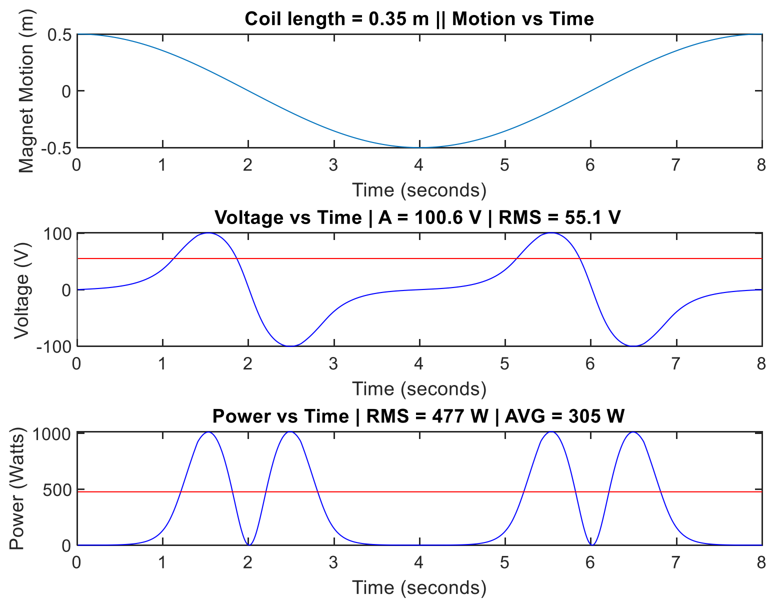

Figure 10 - Voltage and power waveform for the highest average power. This happens at a coil length of 0.35 m and a coil outside diameter of 0.54 m

The waveform with the highest average power is somewhere in between the waveforms shown in Figure 9. According to Figure 8 this configuration leads to a relatively low ratio of peak to RMS value. More research is required to determine if further reducing this ratio is worth the power loss.

4.2 Alternative Magnet Configurations

Other magnet configurations have been evaluated to optimize the wave energy converter output, which were then compared with the currently used configuration. To do so, five magnets with cubic shape and 2 in edges were arranged in four different manners: same polarity along the

r-direction, Halbach array, alternating polarity, and same polarity along the *z*-direction, which is the one that has been used so far.

<u>Same Polarity Along the Long Direction</u>

This magnet arrangement is the one that has been used in the prototype and for the parameter analysis. The magnet arrangement, the magnetic field, and the magnetic flux induced in the coil by the magnet configuration are shown in Figure 11.

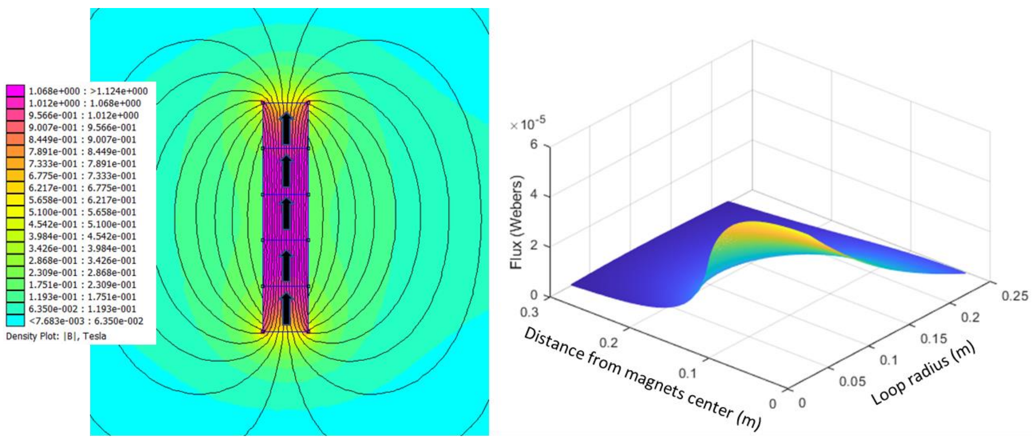

Figure 11 - Same polarity along the z*-direction. The picture on the left displays the magnet arrangement and the magnetic field density. The black arrows point at the magnetic north of each magnet. The picture on the right shows a plot of the magnetic flux through coil loops of different radius and at different* z *distances from the center of the magnets.*

The configuration shown in Figure 11 concentrates the magnetic field lines around the magnets in an axially symmetric manner. Given the coil arrangement, the magnetic flux is maximum when the vertical center of the coil is aligned with the vertical center of the magnets. This magnet configuration is to be compared with three alternative configurations.

<u>Same Polarity Along the *r*-Direction</u>

This is the first alternative arrangement to be considered. Figure 12 shows how the magnets are arranged for the same polarity along the *r*-direction.

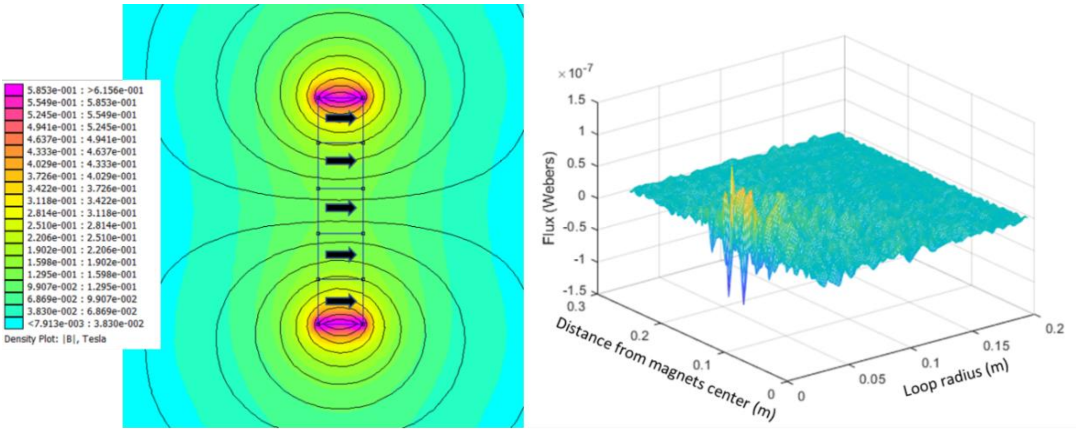

Figure 12 - Same polarity along the r*-direction. The picture on the left displays the magnet arrangement and the magnetic field density. The black arrows point at the magnetic north of each magnet. The picture on the right shows a plot of the magnetic flux through coil loops of different radius and at different* z *distances from the center of the magnet in the vertical direction.*

It can be observed that this magnet configuration organizes the magnetic field lines in a circular manner around the top and bottom extremes of the magnet arrangement. However, the plot that displays the magnetic flux through loops looks noisy, irregular, and the magnitude is small. To better explain this, it is helpful to look at the magnetic field lines and realize that the magnetic field lines on one side of the magnets go in the opposite direction than the lines on the opposite side. Given that the shape of the magnetic field lines is symmetric with respect to the center vertical plane, the resulting magnetic flux through the coil loops is 0. To prove this premise, the magnetic flux from the center plane to different *r* distances at either side of the magnets was plotted. This is shown in Figure 13.

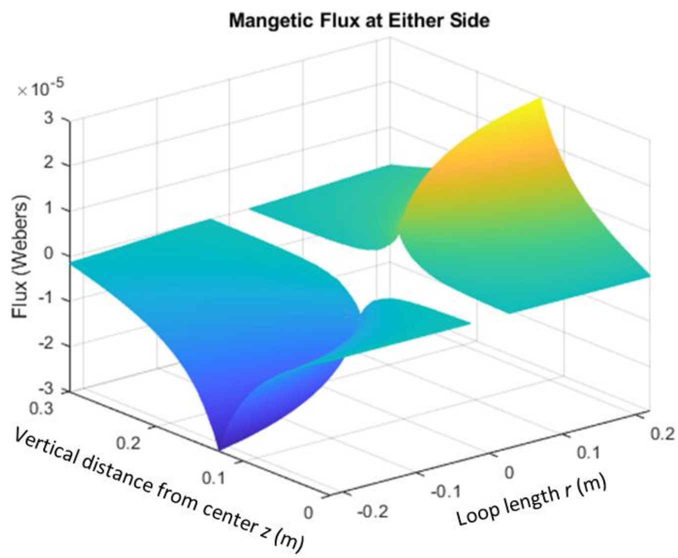

Figure 13 – Two-sided magnetic flux for the same polarity along the r*-direction. The plot shows the magnetic flux through coil loops from the center of the magnet to distance r and vertical distance* z *at both sides of the magnets*

Figure 13 shows that the magnetic flux at either side of the magnet configuration have the same magnitudes with opposite signs. This proves the previously mentioned premise and shows that this configuration is not suitable for the coil configuration that is being used in the wave energy converter.

Alternating Polarity

Alternating polarity is the magnet configuration that, as shown in Figure 14, has the magnets placed with the magnetic field in the opposite direction than the contiguous magnets.

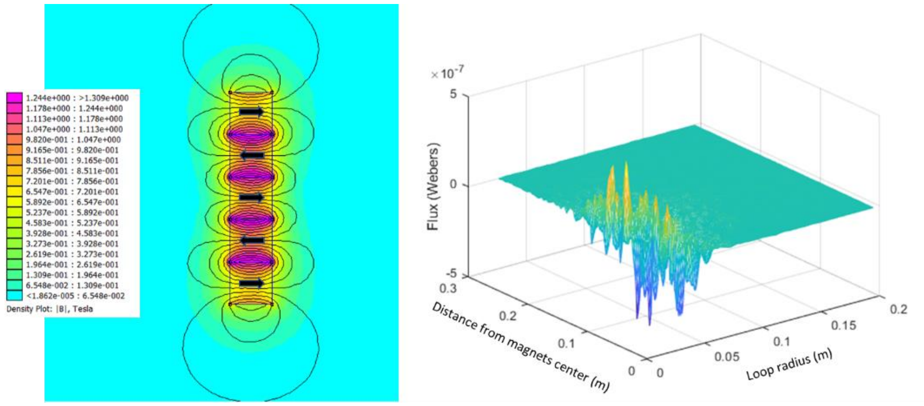

Figure 14 – Alternating polarity. The picture on the left displays the magnet arrangement and the magnetic field density. The black arrows point at the magnetic north of each magnet. The picture on the right shows a plot of the magnetic flux through coil loops of different radius and at different z *distances from the center of the magnet in the vertical direction.*

The magnetic flux plot and the arrangement of the magnetic field lines in Figure 14 show that alternating polarity may, similarly to the configuration of the same polarity along the *r*-direction, induce a negligible output in the coil, due to the opposite direction of the magnetic field lines at either side of the magnets. To confirm this, the magnetic flux from the center plane to different *r* distances at either side of the magnets was plotted in Figure 15.

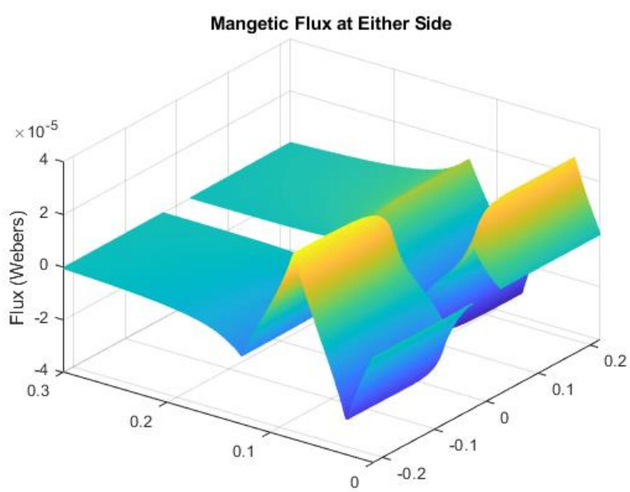

Figure 15 - Two-sided magnetic flux for the same polarity along the r*-direction. The plot shows the magnetic flux at coil loops from the center of the magnet to distance* r *and vertical distance* z *at both sides of the magnets*

As shown in Figure 15, the magnetic flux at either side of the magnets has the same magnitude with opposite signs. Because of this, the resulting output in the current coil configuration would be zero.

<u>Halbach Array</u>

Halbach array is the last alternative configuration to be evaluated. The magnet arrangement, the magnetic field lines distribution, and the magnetic flux through loops of different radius at different distances from the vertical center of the configuration are shown in Figure 16.

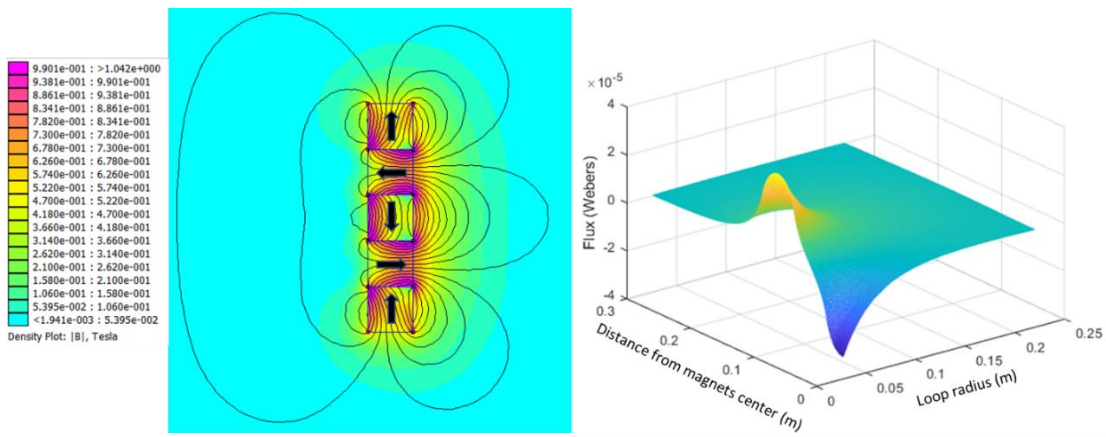

Figure 16 - Halbach array. The picture on the left displays the magnet arrangement and the magnetic field density plot. The black arrows point at the magnetic north of each magnet. The picture on the right shows a plot of the magnetic flux through coil loops of different radius and at different z *distances from the center of the magnet in the vertical direction.*

As shown in Figure 16, the Halbach array is a configuration that maximizes the magnetic field on one side of the magnet configuration. Given the changes in polarity that this configuration creates, the magnetic flux also varies from positive to negative. This configuration creates *n – 2* spikes in the magnetic flux, where *n* is the number of magnets. Since five magnets are being used in this case, there are three sign changes in the magnetic flux throughout the

length of the magnet configuration. This is beneficial for generating electricity since what induces electricity is the change in magnetic flux.

However, because the spikes generated by the magnetic flux are short in the *z*-direction, the coil length must also be small. Otherwise, the spikes will cancel each other out, and lead to a negligible output. One way that this configuration could be useful is by splitting the coil into smaller independent coils whose length in the *z*-direction allow them to use the spikes shown in Figure 16. Using a single coil and changing only the coil length, this configuration led to a maximum of 34% of the maximum average power output obtained using the configuration of the same polarity along the *z*-direction.

After evaluating all four magnet arrangements it can be concluded that same polarity along the *z*-direction provides the best performance. Using concentric coils for alternating polarity and same polarity along the *r*-direction results in a negligible magnetic flux across the coil. Also, Halbach array provides a lower output compared to same polarity along the *z*-direction.

4.3 Coil Configuration

The coil was evaluated to find potential ways to improve the output of the wave energy converter. The first that was evaluated in the coil is the type of winding used, which may be divided as wild or organized winding. Wild winding occurs when the loops of the coil are placed randomly in the coil space. This type of winding is inefficient in occupying the coil space. On the other hand, an organized winding has the loops of the upper layer carefully placed on the grooves created by the layer below, obtaining a more efficient use of the coil space, and leading

to greater output. Figure 17 shows how organized winding looks and how wild winding was modeled in the simulation.

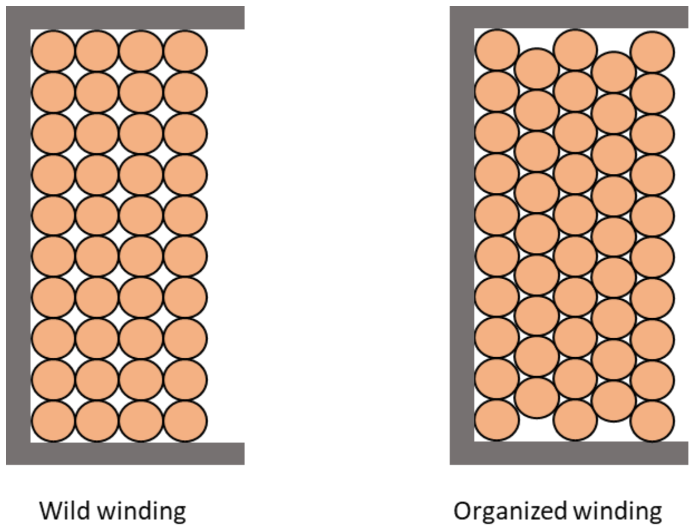

Figure 17 - Representation of how wild and organized windings were modeled in the simulation. The wild winding was modeled as displayed on the left side, and organized winding was modeled as shown on the right side

Given how wild winding was modeled in the simulation, the winding types should not affect the output based on the coil length. However, they should change the output based on the coil outside diameter. Simulations have been run using both types of winding, and a comparison for the voltage and power output at different coil outside diameters is shown in Figure 18.

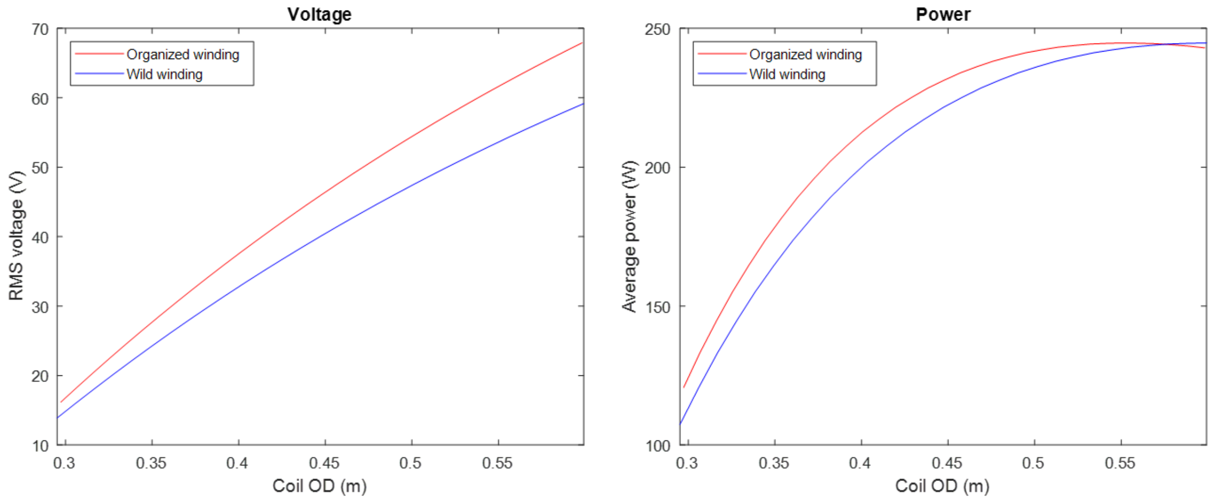

Figure 18 – RMS voltage and average power vs. coil outside diameter for organized and wild winding

As can be observed in Figure 18, the organized winding provides a higher output voltage and power. This is more evident for the voltage plot, where the difference increases as the coil outside diameter increases. For power, using organized winding allows obtaining the maximum power with a smaller outside diameter, allowing for better use of space.

An alternative coil configuration was evaluated to improve the final output. While the current coil is located at the center of the piston motion, this alternative configuration consists of 2 separate coil sections located near the top and bottom ends of the piston motion, as shown in Figure 19. Both coils are at the same distance from the center of motion of the magnet.

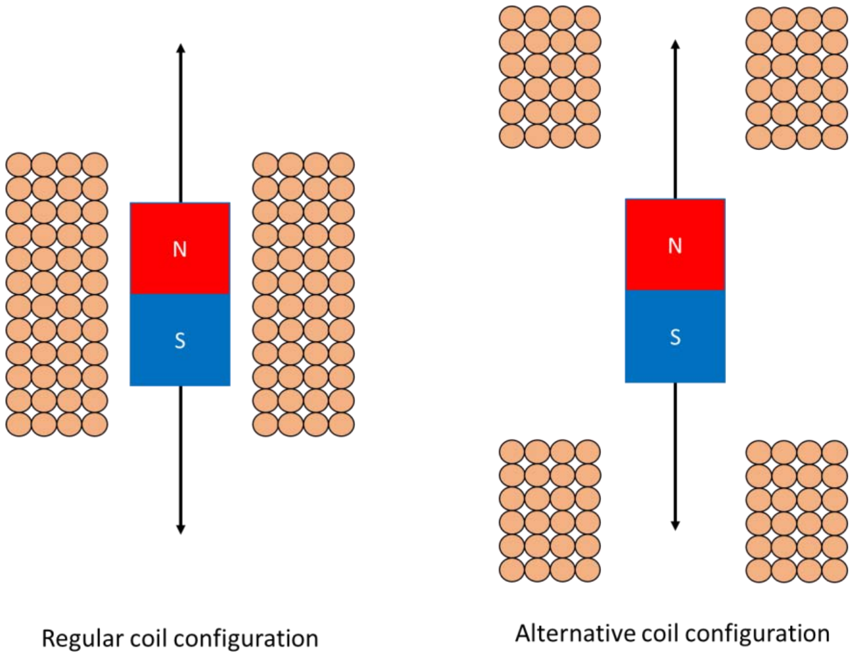

Figure 19 - Comparison between the regular and the alternative coil configuration

Depending on the distance between the coils, they should provide 4 or 8 points of voltage generation along a full wave. Depending on the distance between the separate coils, this configuration could help increase the effectivity of the wave energy converter at different wave heights. Figure 20 shows how the average output power varies with the distance between the coils, assuming that the coils work completely independently from each other.

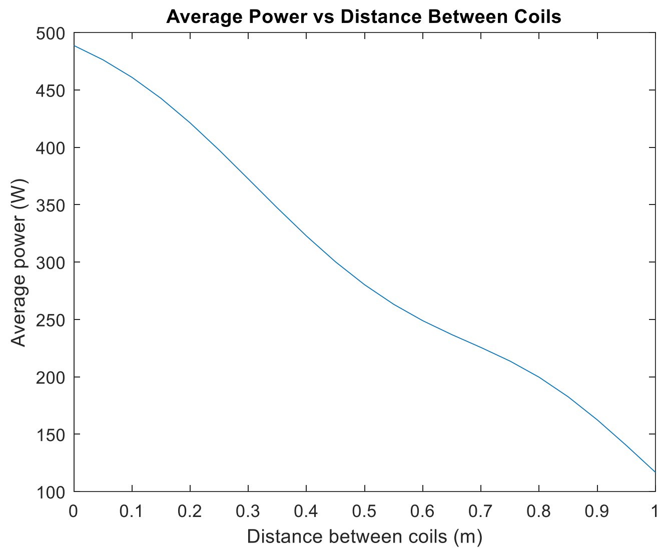

Figure 20 - Average power output vs. distance between the coils. Both coils are at the same distance from the center of motion of the magnets

As shown in Figure 20, the maximum average power is obtained when the distance between the coils is minimum (i.e., when the coils are next to each other). It can also be observed that the output average power is considerably greater than that for the single coil. Assuming that the coils do not influence each other, this could be a great way to boost the overall output power. Further research is required to determine the influence that the separate coils would have on each other. Experimentation is required to determine the real influence that subdividing the coil into two or more independent sections has on the overall output.

4.4 Local Data

To find realistic output data for the wave energy converter, wave height and wave period data from different locations have been analyzed to estimate the output of the wave energy converter at those locations. For this purpose, a single coil with organized winding, a length of 0.34 m, and an outside diameter of 0.54 m were used. To estimate the output of the wave energy converter at the location, the output power of the wave energy converter was calculated for every

H-T combination. The final average power is the result of the weighted sum of each combination's output, where the weight is obtained from the histograms. The locations from which data were obtained are Hawaii, Puerto Rico, Florida, and Alabama.

Hawaii

To study an isolated location in the Pacific Ocean, wave height and wave period data were obtained from Maui, Hawaii. Figure 21 shows histograms of wave height and wave period from 2011 to 2020, about 13 km off the coast of Maui, at a water depth of 200 m. Because the wave energy converter is meant to be at a water depth of about 30 m, the wave height data was shoaled to a water depth of 30 m. Since the data is non-directional, refraction was disregarded.

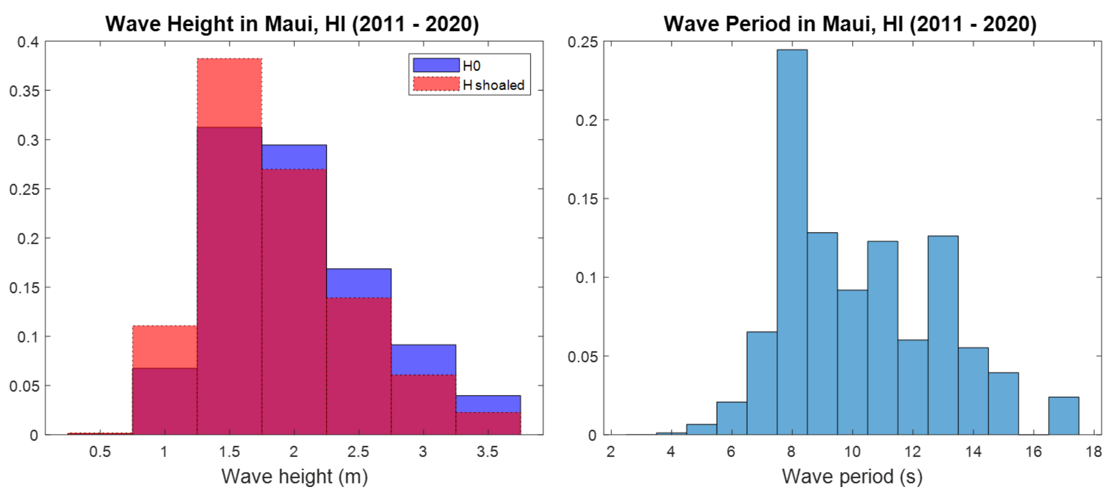

Figure 21 - Histograms of wave height and wave period in Maui, Hawaii, recorded by station 51205 of the NDBC from 2011 to 2020

It can be observed in Figure 21 that shoaling causes wave height to decrease slightly, and the most frequent wave height after shoaling is about 1.5 m. The wave period histogram shows that waves at this location have a wide variety of periods, where 8 seconds is the most frequent period. Using the wave height and period data shown in Figure 21, the wave energy converter provides an average of 0.93 kW, delivering a total of 8 MW·h per year.

Puerto Rico

Data from Ponce, located on the south coast of Puerto Rico, was obtained to study an isolated location in the Atlantic Ocean. Figure 22 shows histograms of wave height and wave period from 2009 to 2020, about 12 km off the coast of Ponce, and 1 km off Isla Caja de Muertos, at a water depth of 18.9 m.

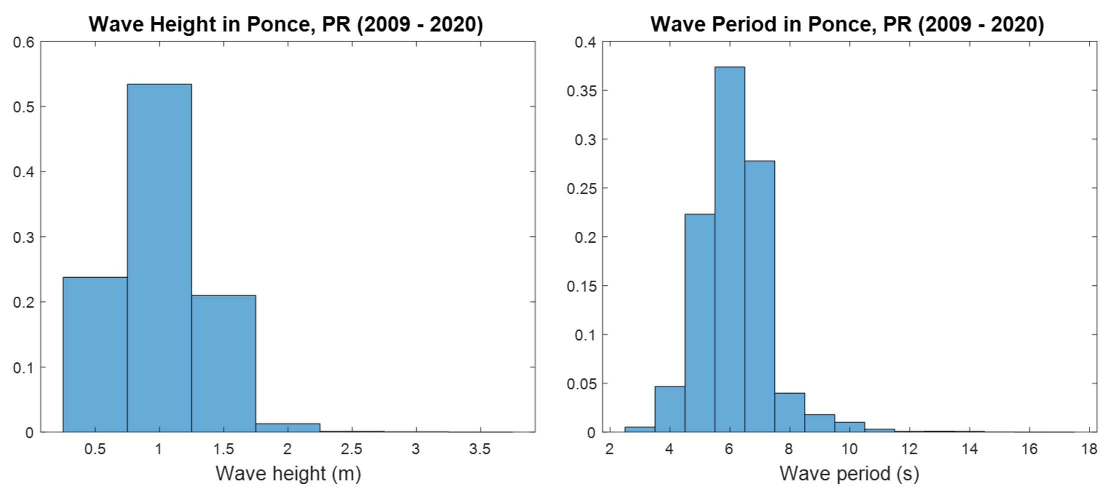

Figure 22 - Histograms of wave height and wave period in Ponce, Puerto Rico, recorded by station 42085 of the NDBC from 2009 to 2020

The histograms of Figure 22 show that the waves at Ponce have a smaller size, with nearly all waves being smaller than 2 m. Also, more than 90% of the waves have a period shorter than 8 s. The waves described by these histograms provide an average of 1.8 kW of power, which yields 16 MW·h per year. This is the greatest output shown so far, led by the short period.

Florida

Fort Pierce, located on the east coast of Florida, was chosen as a representative of the east coast of the United States. Figure 23 shows histograms of wave height and wave period from 2006 to 2020, about 6 km off the coast, at a water depth of 16.5 m.

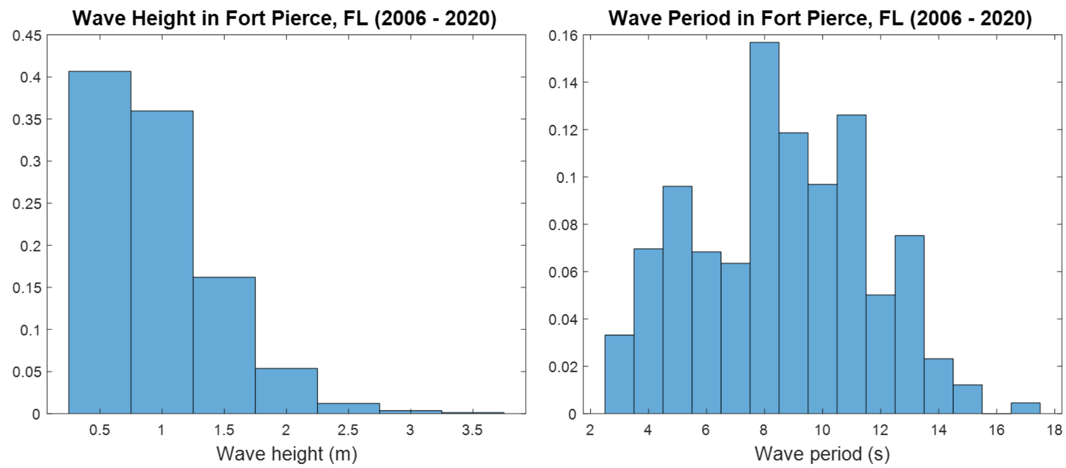

Figure 23 - Histograms of wave height and wave period in Fort Pierce, Florida, recorded by station 41114 of the NDBC from 2006 to 2020

Figure 23 shows that Fort Pierce has a smaller average wave height than the previous locations, with nearly 80% of the waves being under 1.5 m, and the most common wave periods range from 5 to 13 s, with the average wave period being over 8 s. This data leads to an average of 1.4 kW, providing a total of 12 MW·h per year. This is between the power obtained in Hawaii and Puerto Rico.

Alabama

Orange Beach, in the south of Alabama, was chosen as a representative of the coast of the Gulf of Mexico. Figure 24 shows histograms of wave height and wave period from 2009 to 2020, about 20 km off the coast at a water depth of 26 m.

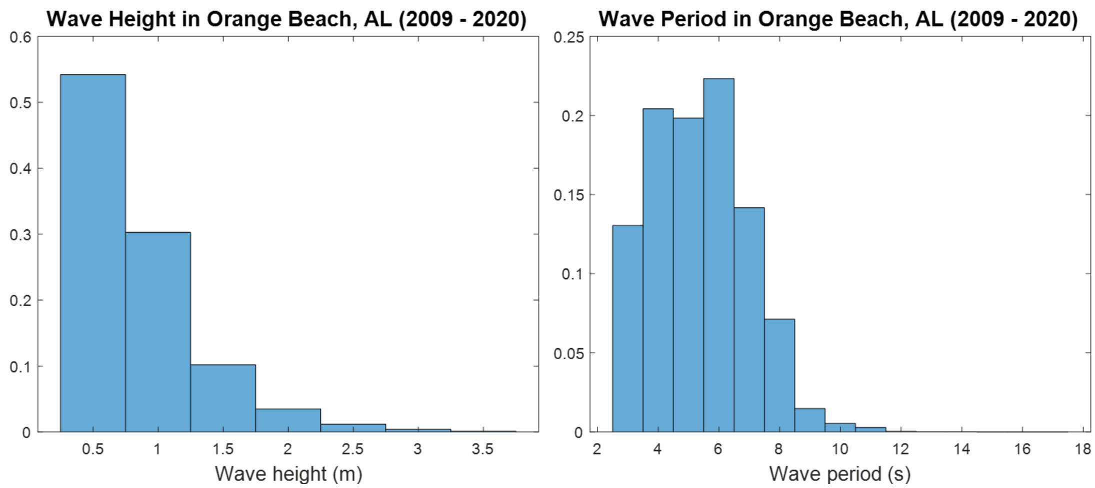

Figure 24 - Histograms of wave height and wave period in Orange Beach, Alabama, recorded by station 42012 of the NDBC from 2009 to 2020

Figure 24 shows that waves in Orange Beach are the smallest of all the observed locations. However, the period is also the shortest at this location, where more than 90% of the waves have less than 7 s period. These waves provide an average of 2.94 kW, providing a total of 26 MW·h per year. This is the highest output of all the studied locations.

After evaluating the performance of the wave energy converter, it can be stated that this energy conversion performs best where waves have a small period, which usually happens at locations with smaller waves. Since this wave energy conversion method does not need significant mechanical components and performs best where ocean conditions are less harsh, this wave energy conversion method is a great choice for cost-efficient devices.

5 Conclusion

This study evaluated the influence that different parameters have in a point absorber wave energy converter that uses linear induction as an energy conversion method. The optimal coil length and coil outside diameter must be determined based on the number and the dimensions of the magnets being used, as well as the expected wave height in the area. The

optimum magnet arrangement for the coil configuration used was determined to be the same polarity along the *z*-direction. It was also determined that using several independent coils may help improve the output and that the optimum operating conditions for this type of wave energy converter are those where the wave period is short. Wave height has a minor influence on the output of the wave energy converter if compared to the wave period.

6 Future Work

Linear generators and wave energy conversion are complex topics that may be further developed. Therefore, the following tasks are suggested to continue this study: (1) determine if reducing the difference between peak and RMS voltage is worth the power loss; (2) further research the influence that contiguous independent coils have on each other; (3) set up an experiment to determine how subdividing the coil into two or more independent sections influences the overall output; (4) implement real physics that include weight, friction, buoyancy, inertia, and size of the floater compared to the wavelength to better determine which wave conditions are best for this type of wave energy conversion; (5) normalize the results so they may be used with other experimental profiles; (6) expand the concept to wave spectra to obtain a more realistic wave input

7 References

Aderinto, Tunde & Li, Hua. (2018). *Ocean Wave Energy Converters: Status and Challenges.* https://www.researchgate.net/publication/325149079_Ocean_Wave_Energy_Converters_Status_and_Challenges

Astariz, S., Iglesias, G. (2015). *The Economics of Wave Energy: A Review.* https://www.sciencedirect.com/science/article/pii/S1364032115000714?via%3Dihub

Cutnell, J. D., & Johnson, K. W. (2012). *Physics*. Hoboken, NJ: Wiley.

Meeker, D. (2019). *FEMM* Version 4.2 [Computer software]. https://www.femm.info/

Edenhofer, O., Madruga, R. P., Sokona, Y. (2013). *Renewable Energy Sources and Climate Change Mitigation: Special Report of the Intergovernmental Panel on Climate Change*. Cambridge University. https://www.ipcc.ch/site/assets/uploads/2018/03/SRREN_Full_Report-1.pdf

EIA (U.S. Energy Information Administration). (2009). *U.S. Energy Consumption by Energy Source, 2005 - 2009*. https://www.eia.gov/renewable/annual/trends/pdf/table1_1.pdf

EIA (U.S. Energy Information Administration). (2019) *Independent Statistics and Analysis*.. https://www.eia.gov/energyexplained/renewable-sources/

Intergovernmental Panel on Climate Change. (2012). Renewable Energy Sources and Climate Change Mitigation. https://archive.ipcc.ch/pdf/special-reports/srren/SRREN_FD_SPM_final.pdf

Koca, K., Kortenhaus, A., Oumeraci, H., Zanuttigh, B., Angelelli, E., Cantù, M., Franceschi, G. (2013, September). *Recent Advances in the Development of Wave Energy Converters.* https://www.researchgate.net/publication/258221898_Recent_Advances_in_the_Development_of_Wave_Energy_Converters.

Liu, Z., Han, Z., Shi, H., & Yang, W. (2017, December). *Experimental study on multi-level overtopping wave energy convertor under regular wave conditions.* https://www.sciencedirect.com/science/article/pii/S209267821730078X

MATLAB. (2019). Version 9.7.0.1190202 (R2019b) [Computer software]. Natick, Massachusetts: The MathWorks Inc.

Polinder, Henk & Mueller, Markus & Scuotto, Mattia & Prado, M.. (2007). *Linear generator systems for wave energy conversion*. Proceedings of the 7th European Wave and Tidal Energy Conference, Porto.

Poullikkas, Andreas. (2014). *Technology prospects of wave power systems*. Electronic Journal of Energy & Environment.

Simone, D.J., (2014). *Modeling a Linear Generator for Energy Harvesting Applications.* https://apps.dtic.mil/dtic/tr/fulltext/u2/a620741.pdf

U.S. Census Bureau. (2020, July 23). *Coastal areas*. https://www.census.gov/topics/preparedness/about/coastal-areas.html#:~:text=Eighty%2Dseven%20million%20people%2C%20or,an%20increase%20of%2040%20million.

U.S. Department of Energy. (2019). *Powering the Blue Economy*: *Exploring Opportunities for Marine Renewable Energy in Maritime Markets*. https://www.energy.gov/sites/prod/files/2019/03/f61/73355.pdf